

# **Aerosol and Cloud feedbacks on Surface Energy Balance over selected regions of Indian subcontinent**

Gayatri Urankar<sup>1\*</sup>, Prabha T.V<sup>1</sup>, Pandithurai G<sup>1</sup>, Pallavi P<sup>1</sup>, Achuthavarier D<sup>2</sup>, Goswami B.N.<sup>1</sup>

1 Indian Institute of Tropical Meteorology, Pune, India

2 Center for Ocean-Land-Atmosphere Studies, Calverton, USA

Address for correspondence:

\*Gayatri Urankar, Indian Institute of Tropical Meteorology,

Dr. Homi Bhabha Road, Pashan, Pune 411008, India.

Email: [gayatri@tropmet.res.in](mailto:gayatri@tropmet.res.in)

## **Abstract**

We investigate aerosol and cloud forcing on the surface energy balance over selected regions in India. Four regions were selected with different surface characteristics and have considerable differences in the long term trends, seasonal distribution of clouds and aerosols. These regions are described as (1) Northern semi-arid, (2) Humid subtropical, (3) Populated central peninsula, and (4) North-east monsoon impacted. Modern Era Retrospective-analysis for Research and Applications (MERRA) data and climate forecast system Reanalysis version 2 (CFSR) data are used in this study. An inter-comparison of cloud fractions from both datasets shows that CFSR systematically underestimates high cloud fraction during pre-monsoon and monsoon seasons. However, there are fewer low cloud fraction biases. The positive temporal trend over 31 years (1979-2009) from MERRA in high clouds is greater than that of low clouds. This is due to positive anomalies in the cloud ice and super cooled liquid water content in the MERRA. Biases in the radiative fluxes and surface fluxes show a strong relationship (correlations exceeding 0.8) with cloud fraction biases, more so for the high clouds. During the pre-monsoon season, aerosol forcing causes a change in surface shortwave radiation of  $-24.5$ ,  $-25$ ,  $-19$  and  $-16 \text{ Wm}^{-2}$  over the above regions 1-4, respectively. The corresponding longwave radiation decrease is  $-9.8$ ,  $-6.8$ ,  $-4.5$  and  $-1.9 \text{ Wm}^{-2}$  over these same regions, respectively. The maximum surface shortwave reduction due to clouds, which is observed during the monsoon season, is  $-86$ ,  $-113$ ,  $-101$  and  $-97 \text{ Wm}^{-2}$ , for these same regions, respectively. A decreasing trend in the boundary layer height is noticed both in MERRA and CFSR. Variation in the Bowen ratio and its relation to aerosol and cloud effect anomalies is also discussed.

## **1. Introduction**

The changes in the net incoming solar radiation and net outgoing radiation at the surface due to anthropogenic activities affect the strength of the hydrological cycle [Trenberth, 1999; Ramanathan *et al.*, 2001; Ramanathan *et al.*, 2005; Wild *et al.*, 2004; Andrews *et al.*, 2008; Wild *et*

*al* 2008; *Liepert and Previdi* 2009]. Several studies [*Allen and Ingram* 2002; *Liepert et al.*, 2004; *Andrews et al.*, 2009] have indicated that radiation forcing is more effective in altering the intensity of hydrologic cycle than thermal forcing due to changes in the greenhouse gases. Numerical modeling studies have also suggested that aerosols in the atmosphere can affect water cycle by altering the regional energy balance in the atmosphere and at the Earth's surface by modulating cloud and rain processes [*Ramanathan et al.*, 2001; *Rosenfeld et al.*, 2008]. Many recent studies have documented variations in aerosol loading, surface cooling and their possible relationships with rainfall in the monsoon regions of India and East Asia [*Krishnan and Ramanathan*, 2002; *Menon et al.*, 2002; *Lau et al.*, 2006; *Huang et al.*, 2006]. Solar dimming over India has been studied by several authors [*Padmakumari et al.*, 2007; *Padmakumari and Goswami*, 2010; *Badrinath et al.*, 2010; *Soni et al.*, 2011]. *Padmakumari and Goswami* [2010] showed that the contribution to the all sky dimming rate ( $-0.89 \text{ W m}^{-2}$  per year) from clouds ( $-1.19 \text{ W m}^{-2}$  per year) is twice as large as that from the aerosols ( $-0.61 \text{ W m}^{-2}$  per year).

Most of the numerical models are unable to account for observed dimming and brightening effects [*Wild and Liepert* 2010]. In the recent reanalysis products such as (Modern Era Retrospective-analysis for Research and Applications; MERRA), aerosol and cloud effects could be isolated. How the total surface energy balance (including the radiation balance) responds to cloud and aerosol forcing is of interest in this study. Clouds produce more cooling effect in shortwave band and warming effect in longwave band for which both middle and high clouds contribute more to shortwave cloud radiative forcing. Over the monsoon region, large areas of high clouds with enhanced optical depth are found [*Balachandran and Rajeevan* 2007]. Also, large negative forcing occurs in regions with large amounts of optically thick high clouds [*Rajeevan and Srinivasan* 2000]. Though radiation budget over the region has been studied, the modulation of total energy budget due to external forcing such as the presence of clouds and aerosols has not been documented over Indian region. Especially, effects on different components of energy balance and the boundary

layer characteristics are not investigated. Studies also suggest that aerosols may impact land surface response on the surface energy balance [*Hollinger et al. 1994; Niyogi et al. 2004*]. These aerosol effects are explicit in the surface fluxes.

Several observational campaigns were carried out in India, focusing on the understanding of energy balance and boundary layer characteristics, for example, Monsoon Trough Boundary Layer Experiment (MONTBLEX) in 1990 [*Narasimha et al., 1997*], Land Surface processes Experiment (LASPEX) during 1997-98 [*Vernekar et al., 2003*]. *Bhat and Arunchandra* [2008] measured energy balance over Bangalore, India was the first experiment carried out in India that addressed the surface energy balance on seasonal time scale. However studies on long term surface energy budget over the Indian subcontinent are lacking. Also, long term observational data is not available for sufficient duration for any verification studies. This situation demands that intercomparison of different datasets also be carried out.

Present study aimed at partially filling this gap, utilizing some of the long period datasets available from satellite derived products (Modern Era Retrospective-analysis for Research and Applications; MERRA). Main objective of the study is to investigate the cloud and aerosol effect on the surface energy budget using MERRA dataset. Second objective is to compare it with the Climate Forecast System Reanalysis dataset (CFSR) which does not include the effect of aerosols explicitly. Reanalysis products are used to study climatic variability and trends. The reanalysis products are typically also used as a forcing for the land surface models to estimate surface fluxes. Thus it is important to investigate the energy balance components in the two recently introduced reanalysis products. This study examines the energy budget at selected regions over India which has distinct aerosol and cloud characteristics. We analyzed the time series of shortwave, longwave, high and low cloud fraction, surface fluxes, and planetary boundary layer height to study inter-annual variability in both datasets (MERRA and CFSR). The CFSR biases were also estimated and their inter relationship with low and high cloud cover was also examined.

## **1. Data and Methods:**

### **2.1. MERRA Data:**

Modern Era Retrospective-analysis for Research and Applications (MERRA) 2D data is used in this study. It is a National Aeronautics and Space Administration (NASA) atmospheric reanalysis project based on a new version of the Goddard Earth Observing System Data Assimilation System Version 5 (GEOS-5), with the adoption of a joint analysis with the National Centers for Environmental Prediction (NCEP) and of a new set of physics packages for the atmospheric general circulation model (AGCM). MERRA focuses on historical analyses of the hydrological cycle on a broad range of weather and climate time scales. MERRA data is available from 1979 through present. For this study we used data from 1979 to 2009. The analysis performed at a horizontal resolution of  $2/3$  degrees longitude by  $1/2$  degree latitude and 72 vertical levels, extending to 0.01 hPa. Detailed documentation of the data access and procedures can be found at <http://gmao.gsfc.nasa.gov/MERRA>. This dataset provides, net downward shortwave (SW) flux, and net downward longwave (LW) flux, for clear sky (no clouds), clean sky (no aerosols) and clean clear sky (no aerosols and no clouds). Aerosol monthly climatology in MERRA is derived from Colarco et al., (2010) and includes dust, sea salt, carbonaceous aerosols, sulfate, etc. It also provides surface turbulent fluxes like sensible heat flux (H), latent heat flux (LH) and ground heat flux (G). Cloud fractions for low and high level clouds (in percent), planetary boundary layer height (in meters) are also used. In MERRA data clouds heights are same as ISCCP. High clouds are those which are above 400 hPa, mid level clouds are between 700 – 400 hPa and low clouds have cloud tops below 700 hPa. High cloud fraction includes convective clouds when appropriate. High cloud and low cloud fraction datasets are also used in this study. This study used monthly average data over whole Indian region ( $6^{\circ}\text{N}$ - $35^{\circ}\text{N}$  and  $68^{\circ}\text{E}$ - $97^{\circ}\text{E}$ ) and detailed study is done over selected locations as described below, for a period of 31 years.

### **2.2. Climate Forecast System Reanalysis Data:**

The National Center for Environmental Prediction (NCEP) Climate Forecast System Reanalysis version 2 (CFSR) uses NCEP coupled forecast system model [*Saha et al.*, 2010]. It is a global, high resolution coupled atmosphere-ocean-land-surface-sea ice system to provide the best estimate for the 31-yr period from 1979 to 2009. New features of CFSR include (1) coupling of atmosphere and ocean during the generation of the 6 hour guess field, (2) an interactive sea-ice model, and (3) assimilation of satellite radiances by the Grid-point Statistical Interpolation (GSI) scheme over the entire period. The CFSR global atmospheric resolution is ~ 38 km (T382) with 64 levels extending from the surface to 0.26 hPa. The global ocean's latitudinal spacing is 0.25 degree at the equator, extending to a global 0.5 degree beyond the tropics, with 40 levels to a depth of 4737 m. The global land surface model has 4 soil levels and the global sea ice model has 3 layers. The CFSR atmospheric model has observed variations in carbon dioxide (CO<sub>2</sub>) over the 1979-2009 period, together with changes in aerosol and other trace gases and solar variations.

### **2.3 Selection of regions:**

Surface Energy budget depends on the climatic condition and surface characteristics such as soil moisture, vegetation, soil type, land use, industrialization, precipitation etc. For this study we have selected four regions of different climates, contrast aerosol and cloud concentrations over Indian subcontinent as shown in Figure 1.

R1: (73-79) E & (22-28) N

R2: (81-86) E & (20-25) N

R3: (75-80) E & (15-20) N

R4: (77-81) E & (10-14) N

R1 is identified as 'Northern semi-arid region' with arid to semi-arid climate where the rate of moisture loss through evapotranspiration exceeds that from precipitation. Summers are exceptionally hot (mean temperature 35° C and daily maxima 45° C) and dry. Average annual rainfall is 730 millimeters (TRMM 1998-2009) and mostly accounted by south-west monsoon.

Maximum rainfall over this region is noticed during July and August months mainly from the westward moving stratiform cloud systems. However, during this period Iran, Afghanistan and Arabia (with the exception of the Arabian Sea coast) remain hot and dry under the influence of Asiatic continental air. This hot dry air and moist air meet and form an Intertropical Front [Sawyer, 1947] and this region is known as transition region. Aerosol optical depth (AOD) varies between 0.4 - 0.5, likely due to dust particle transport from Thar Desert [Habib *et al.*, 2006], long range transport from the middle eastern desert region and also due to other local sources of agricultural burning. Cloud fraction is 0.38 (MODIS TERRA 2000-2009).

Second region R2, identified as 'Humid subtropical', experiences very hot and dry summer (maximum temperature 42 °C) and cold winter (minimum temperature ranges from 4-10 °C). It receives very heavy rainfall (1200 millimeters) during southwest monsoon months (Jun, Jul, Aug, and Sept). Agriculture continues to be of primary importance in this region despite its recent advances in industrial sector due to abundance of natural resources like huge iron ore, coal and mineral reserves etc. Emission of black carbon and inorganic oxidized matter, which is mostly fly ash from coal based power plants, is more in this area. Crop waste, fossil fuel burning contributes to the aerosol load. Annual average AOD varies between 0.3 – 0.4 in this region [Reddy and Venkataraman, 2002a; Ramachandran and Cherian, 2008]. In this region cloud fraction is 0.47.

Third region R3, which can be identified as 'Populated central peninsula' has mainly tropical wet and dry climate with some semi-arid rain shadow region. This has moderate temperatures (maximum temperature is between 30-38 °C and minimum between 18 – 22 °C). The rainy season lasts from June to September; annual rainfall average is 880 millimeter across the region. Population is very dense in this region; the main source for aerosols is biofuel and biomass burning. Also, long range dust transport from Persian Gulf and Arabian Sea region contributes to the pollution [Badrinath *et al.*, 2010]. Annual average of AOD varies between 0.3-0.4 [Reddy and Venkataraman, 2002b; Ramachandran and Cherian, 2008]. Cloud fraction is 0.52 during last 10

years.

Fourth region R4, which is 'North-east monsoon impacted' has tropical wet to semi-arid climate with daily maximum temperatures range between 32 and 43° C. This region gets rain from northeast monsoon occurring during October and November, with annual mean rainfall of 1195 millimeter. The main influence is man-made pollutants and strong presence of sea spray aerosols. Annual average of AOD varies between 0.2-0.3 [Ramachandran and Cherian, 2008] and cloud fraction is 0.67. For this region 8 years of data is missing in MERRA dataset.

## 2.4 Methods:

The surface energy budget equation is given by,

$$Q_* = H + LH + G \quad (1)$$

Where,  $H$  is Sensible heat,  $LH$  is Latent heat and  $G$  is Ground heat flux at the surface.

$$Q_* = Q_{SW} - Q_{LW}, \text{ where } Q_{SW} = SW \downarrow - SW \uparrow \text{ and } Q_{LW} = LW \uparrow - LW \downarrow$$

In Equation 1,  $Q_*$  is positive as a gain and negative when loss, terms on the right hand sides are positive when they represent losses of heat for the surfaces. The exact partitioning of the radiative surplus or deficit is governed by the nature of the surface, radiative abilities of soil and atmosphere through transport of heat.

Aerosol effect is estimated from MERRA data as the difference between clear sky (no clouds but aerosols present) and clean-clear sky (no aerosols and no clouds) radiation components. The cloud effect is defined as the difference in radiation between clean sky (no aerosols but clouds present) and clean-clear sky (no aerosols and no clouds). This aspect is important to determine how much solar radiation gets attenuated by aerosol and clouds. Biases for the low cloud and high cloud fractions and surface fluxes are found from the difference between the CFSR and MERRA datasets.

Bowen ratio ( $B$ ) is defined as the ratio of sensible heat flux to latent heat flux [Stull, 2000]. A value of Bowen ratio greater than one is typically found over surfaces where available water is



limited. On the other hand if  $B$  is less than unity,  $LH$  is greater than  $H$ , and the heat input to the atmosphere is mainly in the latent form. Therefore the climate is likely to be relatively cool and moist. Typical average values for  $B$  are; 0.1 over the sea, 0.2 over irrigated crops, 0.5 over grasslands, 5 over semi-arid regions and 10 over deserts [Stull, 2000].

The present study is organized as follows. Annual surface energy budget over selected regions are described in Section 3.1. Aerosol and cloud effects on incoming and outgoing radiation are discussed in Section 3.2. In Section 3.3, time series of  $SW$ ,  $LW$  fluxes, high and low clouds for MERRA and CFS Reanalysis datasets are compared. Correlation of CFSR cloud fraction bias (high and low level) with the surface fluxes and PBL height biases are discussed in the same section. In Section 3.4 deviation of cloud water and cloud ice mixing ratios are presented for R2 and R3. In the last section 3.5, the effect of aerosols and clouds on Bowen ratio is examined for annual and seasonal aspect. Aerosol and cloud effect anomalies are found by removing the annual cycle from this data and the deviation is found from the difference between original time series and the annual cycle.

### **3. Results and Discussions:**

#### **3.1 Total surface energy budget:**

The average spatial distribution of energy budget components over the period of study from CFSR and MERRA are presented in Figure 2. The spatial distribution of  $SW$  and  $LW$  is similar in both the datasets, while CFSR showed more spatial variations. However  $SH$  and  $LH$  have different energy partition for MERRA and CFSR. MERRA showed long term decreasing trends in the  $SW$ ,  $LW$ , and  $SH$  fluxes and increasing trend in the  $LH$  fluxes over the whole Indian region. CFSR showed no specific trend. Trends in  $SW$ ,  $LW$ , high cloud and low cloud amount are also investigated over Indian region (Figure 3).  $LW$  flux shows increasing trend over Indo Gangetic plain and over coastal areas in both datasets. MERRA data characterize a dimming over the central and east peninsular region. There are strong horizontal gradients in the distribution of  $SW$  trend.

Strong gradients in SW trend are noted over all the four selected regions, from arid, semi arid to moist conditions. In the MERRA data, there is remarkable resemblance between the locations of maximum trends of SW radiation and high cloud amount over land. The negative trend in the MERRA SW extends north westwards over the convergence region.

The energy balance over the selected locations is analyzed using MERRA (1979-2009) dataset. The annual averages of radiative fluxes are presented in Table I. Over R4 region, lower value for net LW is due to higher cloud cover for longer duration compared to other regions; attributed to the coastal effects. The presence of clouds decreases downward SW and hence upward LW. Also, it increases downward LW radiation through reflection and reemission [Devasthale and Grassl, 2009], thus the net LW (outgoing-incoming) flux decreases. On the annual mean basis  $G$  is very small. The partitioning of heat in the form of  $LH$  is more for all regions except for R1 due to the availability of soil moisture. R1 characterizes arid to semi-arid climate with very less precipitation (annual average  $\sim 730$  mm) hence partitioning of available energy to  $LH$  is less and most energy is transferred as  $H$ . Long term annual average cloud fractions are 0.38, 0.47, 0.52, 0.67 and AODs (over 2000-2009 from MODIS) are 0.41, 0.35, 0.36, 0.27 at R1, R2, R3 and R4 respectively.

Monthly variation of surface radiative fluxes for four selected locations averaged over 31 years is presented in Figure 4. Cloud fraction from MERRA data set and AOD from MODIS TERRA (2000-2009) are also presented in the same figure. AOD peaked for R1 region during the month of June and July. The annual cycle of AOD became weaker from R1 to R4. Cloud fraction increased from May to September in R1 region. The distribution of cloud fraction became wider from R1 to R4 with peak during monsoon season. An increase in the cloud fraction over R3 region during pre-monsoon season is mainly associated with thunderstorm events.

Net downward SW radiation at the surface is maximum during the pre-monsoon season (Mar, Apr, May) for all the regions. Net downward SW radiation decreases during the monsoon

season due to increase in cloud fraction and also possibly due to the increased AOD. Net downward  $LW$  radiation (negative values show loss of heat from the surface) increases during pre-monsoon due low cloudiness. Sensible heat ( $H$ ) and ground heat flux ( $G$ ) also show maximum value in pre-monsoon season as they are directly dependent on the incoming solar radiation (latent heat flux ( $LH$ ) is minimum during the pre-monsoon). Maximum incoming radiation is noted in April or in May at all locations except over the coastal region R4. For R1, maximum value of  $SW$ ,  $LW$ ,  $H$  and  $G$  is noticed in the month of May, for R2 and R3 the peak is noted in April while for R4 it is in March.

As soil being dry, sensible heat flux dominates during the pre-monsoon months. Latent heat is more during the monsoon months due to increased rainfall and thus soil moisture content is more.  $LH$  is maximum during June to November at all locations except for the arid region R1. It may be noted that cloudiness over R1 is noticed from June to September, thus precipitation and water available for evaporation are less compared to other regions. Cloudiness over R4 is noticed throughout the year due to the presence of land-sea breeze circulations. Over R4 region,  $LH$  is maximum during October-November, as maximum rainfall is received under the influence of northeast monsoon (60 % of the annual).

In pre-monsoon R1 shows small  $LH$  and  $LW$  is large compared with other locations. Over R4 region this behavior is exactly opposite. R2 and R3 show intermediate characteristics that of R1 and R4.  $LW$  and  $LH$  are negatively correlated. Earth emits  $LW$  radiation, depending on the surface temperature. Similar behavior of the annual cycle of  $LW$  to that of  $SW$  is due to its dependency of surface temperature, which again depends on the net input of energy. In the monsoon months, less amount of  $LW$  is emitted as less amount of  $SW$  reaches the surface due to the presence of clouds. Also the amount of longwave emitted by surface partially depends on  $LH$ . When evaporation takes place, some heat is removed from the surface as  $LH$ , surface cools and upward  $LW$  decreases; additionally, the presence of clouds and aerosols increases the amount of  $LW$  in downward direction (reflection, emission). It is apparent that there is influence of clouds and aerosols over the four

regions, which are distinct with their forcing on the surface energy budget and needs further investigation.

CFSR dataset also shows similar monthly distribution of all the fluxes but values differ from MERRA data. In Figure 5, monthly variations of flux biases (CFSR – MERRA) are presented for energy balance components ( $SW$ ,  $LW$ ,  $H$ ,  $LH$  and  $G$ ). The biases are very high and also show large monthly variations. Bias is less at R4 compared with other regions and maximum over R3 region. CFSR overestimates  $LW$  and  $H$ . It underestimates  $SW$ ,  $LH$  and  $G$  over all the regions. Negative biases in the  $LH$  flux in the CFSR are especially dominant over the R3 region.

### **3.2 Aerosol and cloud forcing/effect:**

Aerosols have a much shorter lifetime (days to weeks) than most greenhouse gases (decades to centuries), and, as a result, their concentrations respond much more quickly to changes in emissions [Houghton *et al.*, 2001]. Consequently, they alter the net radiation by scattering and / or absorbing both at the top and bottom of the atmosphere, causing dimming at the surface, which is the direct effect of aerosols [Ramanathan *et al.*, 2001; Krishnan and Ramanathan, 2002; Huang *et al.*, 2007; Padma Kumari *et al.*, 2007; Panicker *et al.*, 2010]. Such a reduction has been observed in industrial regions of the Northern Hemisphere [Menon, 2002]. Any change in the incoming radiation over a period of time will influence the radiation budget and surface temperature distribution. In order for the surface energy balance to reach a new equilibrium state, the surface energy has to be redistributed which will introduce changes in the components of energy balance.

Figure 6 shows annual cycle of aerosol (for  $SW$  and  $LW$ ) and cloud (for  $SW$ ) forcing averaged over 31 years. The maximum attenuation of the fluxes due to aerosol and cloud forcing is presented in Table II. The negative sign shows a reduction in the received energy at the surface and thus a dimming effect. Aerosols cool the surface by reflecting, scattering and absorbing incoming solar radiation, known as aerosol direct effect. All these regions show maximum attenuation in pre-monsoon, as aerosol loading builds up in this season due to convective and dust

storm activities, forest fires, open burning of crop waste [Ramachandran and Cherian, 2008; Habib *et al.*, 2006]. R1 (AOD  $\approx$  0.45) and R2 (AOD  $\approx$  0.58) show significant effect of aerosols.. In case of R1, dust particles contribute to solar dimming at the surface, air masses carry the dry dust particles from the Middle East and western Thar Desert during pre-monsoon season [Tripathi *et al.*, 2005; Bollasina *et al.*, 2007; Aloysius *et al.*, 2008]. While R2 is highly populated and industrialized regions so it shows strong aerosol effect on SW and LW. Black carbon (BC) absorbs SW radiation, heats the atmosphere and exerts negative forcing at the surface due to a dimming effect. These changes have an additional influence on the thermodynamic structure of the atmosphere which becomes more stable and may resist cloud development [Ramanathan *et al.*, 2005]. On average, BC atmospheric forcing contributes around 55 % of total aerosol atmospheric radiative absorption integrated over all seasons [Panicker *et al.*, 2010]. Region R4 shows smallest value, as this region has much clearer environment (AOD  $\approx$  0.35) compare to other regions. Additionally, this region gets rainfall from both southwest and northeast monsoon thus washout and scavenging influence reduces the aerosol burden [Chate *et al.*, 2003]. We emphasize that aerosol induced dimming effect dominates during the pre-monsoon season R1, R2 and R3 regions. Meanwhile, cloud effect dominates during the monsoon months.

LW aerosol forcing is of comparable magnitude as that of greenhouse gases in warming the earth's surface and in modifying the earth's energy balance [Vogelmann *et al.*, 2003]. Maximum aerosol effect on net LW is in April month over all regions. LW effect over R1 is large compared to other regions due to the presence of dust particles over this region and high AOD ( $\approx$  0.75). Aerosols with coarse particles, such as dust or sea salt can exert direct LW forcing (reflection, scattering and absorption) at the surface [Dufresne *et al.*, 2002; Vogelmann *et al.*, 2003; Lubin and Vogelmann, 2004; Xia and Zong, 2009]. In spite of being a coastal region, R4 does not show large LW forcing. Panicker *et al.* [2008] suggested that about 25 % of the aerosol SW cooling is being compensated by increase in LW radiation ( $8.2 \text{ Wm}^{-2}$ ) due to aerosol absorption and reemission.

These results were derived from ground based observations during December 2004 to February 2005, a short period of time compared to the one presented in the current study. Our results during pre-monsoon season also conform to this finding especially over regions R1 and R2. These studies indicate that higher the aerosol loading, higher is the downward LW flux observed at the surface. This increase reduces the net LW (outgoing-incoming) at the surface.

Clouds reflect the incoming solar radiation (cloud albedo effect) back into the space. Since aerosols act as a cloud condensation nuclei, large number of aerosols create more cloud droplets, which increases reflection of radiation back to space, leading to a net climate cooling (aerosol indirect effect) and may also slow the hydrological cycle [*Ramanathan et al.*, 2001; *Lohmann and Feicher*, 2005; *Huang et al.*, 2006; *Rosenfeld et al.*, 2008]. In Figure 6, reduction in the SW due to the presence of clouds is very large due to the reflection of incoming radiation. Maximum reduction is seen in the monsoon months (JJAS). R2 shows highest attenuation by clouds.

### **3.3 Comparison of MERRA and CFSR datasets:**

A linear regression is carried out on the average low and high cloud fraction during Jan-Dec, pre-monsoon and monsoon periods from MERRA and CFSR and estimates of slopes are presented in Table III (Figure is not shown). Both high and low clouds show positive trend during the past 31 years. MERRA data show increasing trend during Jan-Dec for high cloud fraction 0.23, 0.20, 0.30 and 0.05 per year; and for low cloud fraction 0.07, 0.16, 0.08 and 0.26 per year for R1, R2, R3 and R4 respectively. It is seen that the increase in the annual high-level cloud cover is more than that of low-level cloud cover for all regions except at R4, thus more positive LW feedback at the surface. LW cloud forcing in the tropical region primarily associated with high clouds [*Hartmann et al.*, 1992]. Forcing of the albedo (cooling at the surface) is contributed primarily by clouds with larger optical depth and by low clouds which has negative SW feedback [*Hartmann et al.*, 1992]. Increase in LW flux at the surface can offset SW cooling and warm the earth's surface. The increasing cloud amount during the past 31 years may be due to increasing concentration of aerosols and thus the

indirect effect; as aerosols serve as a CCN, more number of aerosols reduce cloud droplet size hence precipitation efficiency by increasing cloud lifetime [Ramanathan *et al.*, 2001, Huang *et al.*, 2006]. CFSR data also showed the increasing trend in high cloud is more than that of low clouds. However, the rate of increase in the case of CFSR is less in comparison with MERRA data.

A linear regression analysis was done for average SW and LW fluxes over different averaging period; Jan- Dec, pre-monsoon and monsoon season. Estimated slopes are presented in Table IV (Figure is not shown). MERRA-SW flux decreasing trends are -0.48, -0.59, -0.64 and -0.57  $\text{Wm}^{-2}$  per year R1, R2, R3 and R4 respectively. These trends are in general, in close agreement with the SW radiation trends presented by Padma Kumari *et al.* [2007] which are -1.17, -1.28, -0.48 and -0.22  $\text{Wm}^{-2}$  per year for the period 1981- 2004 and Soni *et al.* [2011] found -0.92, -0.87, -0.37 and -0.42  $\text{Wm}^{-2}$  per year for 1971-2005 period at Jodhpur, Kolkata, Pune and Chennai which are the closest stations to the present study. MERRA- LW flux decreasing trends are -0.42, -0.43, -0.41 and -0.39  $\text{Wm}^{-2}$  per year for R1, R2, R3 and R4 respectively. Trend in SW flux is more compared to that of LW flux. CFSR shows negligible decreasing trend for all regions. Decreasing trend in LW (outgoing-incoming; note that MERRA sign convention is followed; where negative value indicates gain at the surface) is attributed to increase in the downward LW at surface due to the presence of aerosols and clouds; this extra greenhouse effect increases surface temperature, resulting in the increased evaporation and fractional cloudiness.

A similar analysis was also carried out for H, LH fluxes and Planetary Boundary Layer (PBL) height and estimated slopes are presented in Table V. Changes in SW and LW can affect the partitioning of heat at the surface. Reduced SW at the surface will reduce H and evaporation (LH). H shows decreasing trend for MERRA data (Jan-Dec) which is -0.59, -0.49, -0.52 and -0.71  $\text{Wm}^{-2}$  per year for R1, R2, R3 and R4 respectively. CFSR shows negligible increasing trend. LH shows increasing trend of 0.52, 0.31, 0.28 and 0.67  $\text{Wm}^{-2}$  per year for R1, R2, R3 and R4 respectively. This increase is may be due to increase in LW at the surface due to enhanced Green House effect by

clouds and aerosols. CFSR shows insignificant trend for LH. Increase in LH and decrease H is more for R4 in MERRA data, attributed to presence more cloud cover over that region.

PBL over land rapidly responds to incoming solar radiation. Heating at the surface will initiate convective mixing and will increase PBL height. Shallow convection derives energy from the boundary layer mixing and their representation in the climate models is closely linked to the PBL characteristics. This is important since there are significant feedbacks between boundary layer clouds and climate [Stull, 2000]. PBL height shows decreasing trend (-4.48, -3.98, -3.65 and -4.33 m per year) for R1, R2, R3 and R4 respectively in Jan-Dec season. The decrease is due to reduced SW and hence sensible heat at the surface. Trends in CFSR data for PBL are smaller.

### **3.3.1. Model biases in cloud cover and their relationships**

A relationship between the cloud fraction bias (CFSR-MERRA) and bias in the SW, LW, H, LH fluxes and PBL height are presented in Figure 7 for high clouds and in Figure 8 for low clouds. We note that, For Jan–Dec period, high cloud bias is negative except at R4 i.e. CFSR underestimates high clouds for R1, R2 and R3 but overestimates for R4 during all seasons. In case of low cloud fraction, CFSR low clouds bias is very less except for R4 where it underestimates in all seasons. In CFSR product low cloud errors are considerably minimized. CFS forecast model version 1.0 was also compared with MERRA (results are not presented), which showed an overestimation of low clouds and high clouds during pre-monsoon and an underestimation during monsoon. However no such differences in the biases exist for the CFSR data.

Annual SW bias is negative over all regions. In pre-monsoon and monsoon SW bias is negative (it underestimates SW by  $\approx 40 \text{ Wm}^{-2}$ ) except for R4 (where the values are scattered on the both sides of zero). LW bias is also negative for all seasons. In case of H, CFSR overestimates for all regions during Jan-Dec, pre-monsoon and monsoon. CFSR underestimates LH for all regions during all seasons. PBL heights from CFSR are overestimated by approximately 200 m for all regions during Jan-Dec, pre-monsoon and monsoon period. Biases in SW, LW, H and PBL height



decreases with increase in high cloud bias and LH bias decreases with decrease in high cloud bias. Relation of these fluxes with low cloud fraction bias is very less.

Cirrus cloud amount is a dominant high cloud type over the Indian region, approximately 65 % of all cloud grids [*Tang and Chen, 2006*]. It was also noted that the cirrus reflectance from the MODIS data products showed a strong latitudinal dependence (Figure 9). Selected regions fall in the high to low cirrus reflectance regions as indicated in the figure. Hence, it is necessary that good estimation of high cloud fraction in climate models and reanalysis products for the prediction of other fluxes.

SW, LW, H and PBL height biases are negatively correlated and LH is positively correlated with both high and low cloud fraction biases. In pre-monsoon season all parameters are highly correlated to low cloud bias than that of high cloud bias except at R3. In monsoon season, correlation of all parameters (except at R3) with high cloud bias is stronger than that of low cloud bias. The CFSR has higher PBL heights than that of MERRA and PBL bias is well correlated with high cloud fraction biases.

### **3.4 Cloud water and cloud ice mixing ratio**

In Section 3.3, it is seen that increasing trend in high level cloud is more than that of low-level cloud, which is able to explain the bias in the radiation and other surface fluxes. There are studies discussing the indirect effect of aerosols on the cloud microstructure; however consensus on the gross effect of aerosols is still to be uncovered [*Levin and Cotton, 2008*]. Several studies have reported the importance of supercooled liquid in the deep convective clouds [*Rosenfeld and Woodley, 2000; Khain et al., 2001; Fan et al., 2010*] in the presence of high CCN concentrations. Vertical profiles of Cloud liquid water (LWC) and ice water content (IWC) from MERRA dataset is used in this section. The annual cycle of LWC and IWC are removed from the dataset and the anomalies of LWC and IWC are presented in Figure 10 for R2 and R3. LWC anomaly is positive since 1999 over both R2 (a) and R3 (b) at elevated layers. This indicates that super cooled liquid

increased in these regions, more so over R3 region. This may be attributed to more number of aerosol particles present over R3 than R2. One pathway for high liquid water content at elevated layers is through nucleation of aerosol particles at higher levels in the deep convective clouds. This leads to supercooled liquid and is typically observed [Prabha *et al.*, 2011] and modeled in several cloud microphysical studies. The CCN concentration at elevated layers could vary from few hundred to thousand  $\text{cm}^{-3}$ , depending on the location, and the air mass trajectories [Kulkarni *et al.*, 2011]. The other pathway for high liquid water content at elevated layers is that through inhibition of precipitation, where aerosols can increase the cloud liquid water content. High concentration of small cloud droplets decrease the collision-coalescence efficiency hence no homogeneous nucleation takes place and also the scarcity of Ice Nuclei (IN) is one of the reasons [Rosenfeld and Woodley, 2000]. But above that level super cooled water suddenly disappears due to homogeneous freezing, which shows elevated IWC at 200 hPa. This increase in IWC leads to reflection of more LW radiation back to the surface and thus more infrared warming at the surface. Presence of high level supercooled water clouds indicate that, clouds are not precipitating earlier due to increase in the number of small liquid droplets.

Increased cloud ice and cloud water mixing ratio for R3 indicates that, more downward LW radiation reaches the surface over R3 compared to R2. Hence net LW (up – down) decrease for R3 is less than that over R2 as seen in Figure 6. Increase in cloud ice mixing ratio is more compared to cloud water mixing ratio. This may be attributed to increased cloud lifetime and cloud water/ice path could increase the amount of high clouds

### **3. 5. Effect of aerosol (AE) and clouds (CE) on Bowen Ratio (B):**

Figure 11 represents the Bowen ratio relationship with cloud and aerosol effect anomalies. The aerosol or cloud effect anomaly is found by removing the annual cycle (presented in Figure 6) from the estimated monthly values of aerosol or cloud effect. This analysis is carried out to investigate the net effect of aerosol and cloud on the partitioning of the surface fluxes.

In pre-monsoon B is more as H is more than LH. During monsoon, Latent heat flux dominates and B is less. Over annual mean, B is less than 1 at R2, R3 and R4 and more at R1. R1 has an arid to semi-arid type climate and has less soil moisture therefore; value of H is more than LH. Cloud and Aerosol effect anomaly show strong negative correlation with B. As CE or AE decreases, B increases. Decrease in clouds or aerosols allow more radiation to reach the surface hence H increases due to this B increases. Partitioning of heat at the surface changes by increase or decrease in amount of aerosols and/or clouds.

The estimated slopes and correlation coefficients between the aerosol or cloud effect anomaly and Bowen ratio are presented in Table VI. Decrease in aerosols and clouds for all seasons are more for R2 compared to all regions. In monsoon, change in B with AE anomaly is more (-1.24, -3.81, -0.25 and 0.04) compared to pre-monsoon (-0.01, -10.4, -0.04 and -0.16). Similarly, change in CE anomaly with bowen ratio is more in monsoon (-76.35, -151.83, -154.85 and -42.87) than pre-monsoon (-0.16, -45.35, -4.02 and -13.42) for R1, R2, R3 and R4 respectively. Correlation coefficient of B with annual aerosol effect is, - 0.76, -0.75, -0.38 and -0.58; and with cloud effect it is -0.87, -0.84, -0.88 and -0.82 for R1, R2, R3 and R4 respectively. Correlation between B and Cloud effect is stronger than that of aerosol effect. These results indicate that aerosol forcing anomaly is strongly correlated for the northern locations (R1 and R2) where there is a distinct seasonal variation of the aerosol optical depth. This may also result from higher amounts of absorbing aerosols. In the presence of absorbing aerosols, warmer boundary layer with higher albedo modifies the cloud cover and impacts boundary layer moisture, leading to a shallow boundary layer, which further change the surface energy fluxes [Pielke et al. 2002].

#### **4. Conclusions:**

Following conclusions are drawn from the present study.

1. MERRA dataset showed a dimming trend in the SW in the central and north eastern part of peninsular India.

2. Aerosol induced dimming effects dominate during the pre-monsoon season at R1, R2 and R3 regions. Observed dimming due to the presence of aerosols is maximum in pre-monsoon which is  $\approx -24.5$ ,  $-25$ ,  $-19$  and  $-16 \text{ Wm}^{-2}$ , where as due to clouds it is maximum in monsoon  $\approx -86$ ,  $-113$ ,  $-101$  and  $-97 \text{ Wm}^{-2}$ . LW surface warming due to aerosols is found to be maximum in pre-monsoon  $\approx 9.8$ ,  $6.8$ ,  $4.5$  and  $1.9 \text{ Wm}^{-2}$  for R1, R2, R3 and R4 respectively and in conformance with an earlier study [Paniker *et al.*, 2009] that it compensates for the 20-25 % of the SW dimming effect.
3. Both net SW and net LW fluxes from MERRA show decreasing trend during 1979-2009 for all seasons, however CFSR does not show such a trend possibly due to inadequate aerosol representation in CFSR. In comparison with MERRA, CFSR data underestimates SW and LW fluxes in pre-monsoon and monsoon.
4. High and low cloud fraction from MERRA showed increasing trend during all seasons. Trend in high clouds is more than that of low clouds. CFSR underestimates high clouds in comparison with MERRA as a result of significant under prediction of cloud amount during pre-monsoon and monsoon season (except over R4 region). In the case of low clouds, it overestimates low clouds as a result of significant over prediction of low cloud amount during the pre-monsoon and monsoon season (except for R4 region).
5. An analysis of IWC and LWC profiles over two locations indicated that supercooled water increased in the recent years and the IWC also followed a similar behavior at 200 hPa in association with the cirrus cloud cover.
6. PBL height from CFSR is higher (200-600 m) than that of MERRA, and PBL bias is well correlated with the high cloud biases. Low cloud biases are very less compared to high cloud biases.
7. Sensible heat flux from MERRA has a decreasing trend which is  $\sim -0.59$ ,  $-0.49$ ,  $-0.52$  and  $-0.71 \text{ W m}^{-2}$  per year; and latent heat flux showed an increasing trend  $\sim 0.52$ ,  $0.31$ ,  $0.28$  and  $-$

0.67 W m<sup>-2</sup> per year for R1, R2, R3 and R4 respectively. CFSR product shows negligible and insignificant trend for H and LH.

8. Bowen ratio shows strong negative correlation with aerosol and cloud effect anomalies. Thus, as aerosol effect or cloud effect increases B decreases due to less radiation reaching the surface. Correlation between B and cloud effect is stronger than that with the aerosol effect.

Evaluation of energy budget components using direct observations is not addressed in this study due to lack of such long period observations. However, such evaluations could be carried out in short period datasets at a seasonal scale.

## **5. Acknowledgements:**

The authors thank MODIS and The Global Modelling and Assimilation Office (GMAO) and the GES DISC for the dissemination of the MERRA data. CFSR data were developed by the NOAA's National Centers for Environmental Prediction (NCEP). The data for this study are from the Research Data Archive (RDA) which is maintained by the Computational and Information Systems Laboratory (CISL) at the National Center for Atmospheric Research (NCAR). NCAR is sponsored by the National Science Foundation (NFS). We thank Bob Dattore for his help with the CFSR datasets. Two anonymous reviewers and editor Prof. Steven Ghan are thanked for valuable suggestions that lead to improvement of the manuscript.

## **References:**

Allen M. R. and Ingram W. (2002), Constraints on future changes in climate and the hydrologic cycle, *Nature*, 419 224–32

Aloysius M. , M. Mohan, K Parameswaran, S. K. George and P. R. Nair (2008), Aerosol transport over Gangetic basin during ISRO-GBP land campaign-II, *Ann. Geophys.*, 26, 431-440.

- Andrews T., Piers M. Forster and Jonathan M. Gregory (2008), A Surface Energy Perspective on Climate Change, *J. Climate*, DOI: 10.1175/2008JCLI2759.1.
- Badrinath K. V. S., A. R. Sharma, D. G. Kaskautis, S. K. Kharol, and H. D. Kambezidis (2010), Solar dimming over the tropical urban region of Hyderabad, India: Effect of increased cloudiness and increased anthropogenic aerosols, *J. Geophys. Res.*, 115, D21208, doi:10.1029/2009JD013694.
- Badrinath K. V. S., S. K. Kharol, D. G. Kaskautis, A. R. Sharma., V. Ramaswamy, H. D. Kambezidis (2010), Long-range transport of dust aerosols over the Arabian Sea and Indian region – A case study using satellite data and ground-based measurements., *Global Planet Change*, v.72, iss. 3, p. 164-181.
- Balachandran S., and M. Rajeevan (2007), Sensitivity of surface radiation budget to clouds over the Asian monsoon region. *J. Earth Syst. Sci.*, 116, No. 2, 159-169.
- Bhat G. S. and S. C. Arunchandra (2008), On the measurement of the surface energy budget over a land surface during the summer monsoon, *J. Earth Syst. Sci.*, vol 117, No. 6, pp. 911-923.
- Bollasina Massimo, Sumant Nigam and K.M. Lau (2008), Absorbing Aerosols and Summer Monsoon Evolution over South Asia: An Observational Portrayal. *J. Climate*, **21**, 3221–3239.
- Chate D. M., P. S. P. Rao, M. S. Naik, G. A. Momin, P. D. Safai, K. Ali (2003), Scavenging of aerosols and their chemical species by rain, *Atmos. Environ.*, Vol 37, Issue 18, Pages 2477-2484, ISSN 1352-2310, DOI: 10.1016/S1352-2310(03)00162-6.
- Colarco P., Da Silva A., Chin M., and Diehl T. (2010), Online simulations of global aerosol distributions in the NASA GEOS-4 model and comparisons to satellite and ground-based aerosol optical depth. *J. Geophys. Res.*, 115, –. doi:10.1029/2009JD012820

- Devasthale A. and H. Grassl (2009), A daytime climatological distribution of high opaque ice cloud classes over the Indian summer monsoon region observed from 25-year AVHRR data, *Atmos. Chem. Phys. Discuss.*, **9**, 23–58.
- Dufresne J., C. Gautier, P. Ricchiuzzi and Y. Fouquart (2002), Longwave Scattering Effects of Mineral Aerosols, *J. Atmos. Sci.*, Vol: 59, 1959-1966.
- Fan J., Jennifer M. Comstock and Mikhail Ovchinnikov (2010), The cloud condensation nuclei and ice nuclei effects on tropical anvil characteristics and water vapor of the tropical tropopause layer, *Environ. Res. Lett.*, 5(2010) 044005(6pp).
- Habib G., C. Venkataraman, I. Chiappell, S. Ramachandran, O. Boucher and M. S. Reddy (2006), Seasonal and interannual variability in absorbing aerosols over India derived from TOMS: Relationship to regional meteorology and emissions. *Atmos. Environ.*, **40**, 1909-1921.
- Hartmann D., E. Maureen, Ockert-Bell, Marc Michelsen (1992), The effect of cloud type on Earth's energy balance: Global analysis, *J. Climate*, Vol. 5, 1281-1304.
- Hollinger D. Y., Kelliher F. M., Byers J. N., Hunt J. E., McSeveny T. M., Weir P. L. (1994) Carbon dioxide exchange between an undisturbed old-growth temperate forest and the atmosphere. *Ecology*, 75:134–150. doi:10.2307/1939390
- Houghton J.T., Y. Ding, D.J. Griggs, M. Noguer, P.J. van der Linden, X. Dai, K. Maskell, C.A. Johnson (2001), *Climate Change 2001: The Scientific Basis*, Published for the Intergovernmental Panel On Climate Change, Cambridge University Press: New York.
- Huang Y., Robert E. Dickinson and William L. Chameides (2006), Impact of aerosol indirect effect on surface Temperature over East Asia, *PNAS*, vol. 103, 4371–4376.
- Khain, A. P., D. Rosenfeld, and A. Pokrovsky (2001), Simulating convective clouds with sustained supercooled liquid water down to  $-37.5^{\circ}\text{C}$  using a spectral microphysics model, *Geophys. Res. Lett.*, 28(20), 3887–3890, doi:10.1029/2000GL012662.

- Krishnan R. and V. Ramanathan (2002), Evidence of surface cooling from absorbing aerosols, *Geophys. Res. Lett.*, VOL. 29, NO. 9, 1340, 10.1029/2002GL014687.
- Kulkarni, J. R., Maheshkumar, R. S., Morwal, S. B; Padma Kumari, B., Mahen Konwar, Deshpande C. G., Joshi R. R., Bhalwankar R. V., Pandithurai G., Safai P.D., Narkhedkar S. G., Dani K. K., Nath A., Sathy Nair., Sapre V. V., Puranik P. V., Kandalgaonkar S., Mujumdar V. R., Khaladkar R. M., Vijayakumar R., Thara V. P. and B. N.Goswami, 2011, The Cloud Aerosol Interactions and Precipitation Enhancement Experiment (CAIPEEX): Overview and Preliminary Results, under review, *Current Science*
- Lau K.M., M. K. Kim, K. M. Kim (2006), Asian summer monsoon anomalies induced by aerosol direct forcing: The role of Tibetan plateau, *Clim. Dynam.*, Vol. 26, 855–864, DOI 10.1007/s00382-006-0114-z.
- Levin Z. and W. R. Cotton (2008), *Aerosol Pollution Impact On Precipitation: A Scientific Review*, Springer Press.
- Liepert B. G., Feichter J., Lohmann U. and Roeckner E. (2004), Can aerosols spin down the water cycle in a warmer and moister world?, *Geophys. Res. Lett.* 31 L06207.
- Liepert B. G. and Previdi M. (2009), Do models and observations disagree on the rainfall response to global warming?, *J. Climate*, 22 3156–66.
- Lohmann U. and J. Feichter (2005), ‘Global indirect aerosol effects: a review’, *Atmos. Chem. Phys.*, 5, 715–737.
- Lubin D. and A. Vogelmann (2004), Longwave Aerosol Direct and Indirect Radiative Effects at the NSA Site, Fourteenth ARM Science Team Meeting Proceedings, Albuquerque, New Mexico, March 22-26.
- Menon S., J. Hansen, L. Nazarenko, Y. Luo (2002), Climate Effects of Black Carbon Aerosols in China and India, *Science*, 2002 Sep 27; 297(5590), 2250-3.



- Narasimha R, D. R. Sikka and A. Prabhu (1997), The monsoon through boundary layer (Bangalore, India: Indian Academy of Sciences), 422 pp.
- Niyogi D, Chang H et al. (2004) Direct observations of the effects of aerosol loading on net ecosystem CO<sub>2</sub> exchanges over different landscapes. *Geophys Res Lett* 31:L20506 (doi: 10.1029/2004GL020915)
- Padma Kumari B., A. L. Londhe, S. Daniel and D. B. Jadhav (2007), Observational evidence of solar dimming: Offsetting surface warming over India, *Geophys. Res. Lett.*, 34, L21810, doi: 10.1029/2007GL031133.
- Padma Kumari B. and B. N. Goswami (2010), Seminal role of clouds on solar dimming over the Indian monsoon region, *Geophys. Res. Lett.*, 37, L06703, doi: 10.1029/2009GL042133.
- Panicker A. S., G. Pandithurai, P. D. Safai, and S. Kewat (2008), Observations of enhanced aerosol longwave radiative forcing over an urban environment, *Geophys. Res. Lett.*, 35, L04817, doi: 10.1029/2007GL032879.
- Panicker A.S., G. Pandithurai, P.D. Safai, S. Dipu, Dong-In Lee (2010), On the contribution of black carbon to the composite aerosol radiative forcing over an urban environment, *Atmos. Environ.*, 44, 3066-3070.
- Prabha T. V., Khain, A., Maheshkumar, R. S., Pandithurai, G., Kulkarni, J. R., Konwar, M. and Goswami, B. N., Microphysics of pre-monsoon and monsoon clouds as seen from in situ measurements during CAIPEEX. *J. Atmos. Sci.*, 2011, doi: 10.1175/2011JAS3707.1.
- Pielke RA Sr (2002) Mesoscale meteorological modeling, 2nd edn. Academic Press, San Diego
- Rajeevan M., and J. Srinivasan (2000), Net cloud radiative forcing at the top of the atmosphere in the Asian monsoon region, *J. Climate*, 13(3), 650-657.

- Ramanathan V., P. J. Crutzen, J. T. Kiehl and D. Rosenfeld (2001), Aerosols, Climate, and the Hydrological Cycle, *Science*, 294, 2119.
- Ramanathan V., C. Chung, D. Kim, T. Bettge, L. Buja, J. T. Kieh, W. M. Washington, Q. Fu, D. R. Sikka and M. Wild (2005), Atmospheric brown clouds: Impacts on South Asian climate and hydrological cycle, *PNAS*, 5326–5333, vol. 102, no. 15.
- Ramchandran S. and R. Cherian (2008), Regional and seasonal variations in aerosol optical characteristics and their frequency distributions over India during 2001-2005, *J. Geophys. Res.*, 113, D08207, doi:10.1029/2007JD008560.
- Reddy M. S. and C. Venkataraman (2002a), Inventory of aerosol and sulphur dioxide emissions from India: I-Fossil fuel combustion, *Atmos. Environ.*, 36, 677-697.
- Reddy M. S. and C. Venkataraman (2002b), Inventory of aerosol and sulphur dioxide emissions from India: II-Biomass combustion, *Atmos. Environ.*, 36, 699-712.
- Rosenfeld D., and W. L. Woodley (2000), Deep convective clouds with sustained supercooled liquid water down to  $-37.5^{\circ}\text{C}$ , *Nature*, 405, 440–441, doi:10.1038/35013030.
- Rosenfeld D., Ulrike Lohmann, Graciela B. Raga, Colin D. O'Dowd, Markku Kulmala, Sandro Fuzzi, Anni Reissell, and Meinrat O. Andreae (2008), Flood or Drought: How Do Aerosols Affect Precipitation?, *Science*, **321** (5894), 1309. DOI: 10.1126/science.1160606.
- Saha S. et al (2010), The NCEP climate forecast system reanalysis. *Bull. Amer. Meteor. Soc.*, 91:1015-1057.
- Sawyer J. S. (1947), The structure of the intertropical front over N.W. India during the S.W. Monsoon, *Quart. J. Roy. Meteor. Soc.*, 73: 346-369. Doi: 10.1002/qj.49707331709.
- Soni V. K., G. Pandithurai and D. S. Pai (2011), Evaluation of long-term changes of solar radiation in India. *Int. J. Climatol.*, n/a. doi: 10.1002/joc.2294.

- Stull R. B. (2000), *Meteorology for scientists and engineers*, second edition, Brooks/Cole publications.
- Tang Xu and Baode Chen (2006), Cloud types associated with the Asian summer monsoon as determined from MODIS/TERRA measurements and a comparison with surface observations, *Geophys. Res. Lett.*, 33, L07814, doi: 10.1029/2006GL026004.
- Trenberth K. (1999), Conceptual framework for changes of extremes of the hydrological cycle with climate change, in *Climatic Change*, 42: 327-339, Kluwer Academic publishers. Printed in Netherlands.
- Tripathi S. N., Sagnik Dey, A. Chandel, S. Srivastava, Ramesh P. Singh, and B. N. Holben (2005), Comparison of MODIS and AERONET derived aerosol optical depth over the Ganga Basin, India, *Ann. Geophys.*, 23, 1093–1101, 2005.
- Vernekar K. G., S. Sinha, L. K. Sadani, S. Sivaramakrishnan, S. S. Parasnis, Brij Mohan, S. Dharmaraj, M. N. Patil, J. S. Pillai, B. S Murthy., B. Debaje and A. Bagavathsingh (2003), An overview of the Land Surface Processes Experiment (Laspex) over a Semi-Arid Region of India, *Bound-Lay. Meteorol.*, 106, 561-572
- Vogelmann A., Piotr J. Flatau, Malgorzata Szczodrak, Krzysztof M. Markowicz, and Peter J. Minnett (2003), Observations of large aerosol infrared forcing at the surface, *Geophys. Res. Lett.*, VOL. 30, NO. 12, 1655, doi:10.1029/2002GL016829.
- Wild M., Grieser J. and Schär C. (2008), Combined surface solar brightening and increasing greenhouse effect support recent intensification of the global land-based hydrological cycle, *Geophys. Res. Lett.* 35 L17706.
- Wild M. and Beate Liepert (2010), The Earth radiation balance as driver of the global hydrological cycle, *Environ. Res. Lett.* 5, 025203, doi:10.1088/1748-9326/5/2/025203.

Wild M., Atsumu Ohmura, Hans Gilgen and D. Rosenfeld (2004), On the consistency of trends in radiation and temperature records and implications for the global hydrological cycle, *Geophys. Res. Lett.*, VOL. 31, L11201, DOI: 10.1029/2003GL019188.

Xia X., and X. Zong (2009), Shortwave versus longwave direct radiative forcing by Taklimakan dust aerosols, *Geophys. Res. Lett.*, 36, L07803, doi:10.1029/2009GL037237.

Zelinka M. D. and D. L. Hartmann (2010), Why is longwave cloud feedback positive?, *J. Geophys. Res.*, 115, D16117, doi: 10.1029/2010JD0138

**Figure captions:**

Figure 1: Selected study regions over Indian subcontinent.

Figure 2: Spatial distribution of fluxes averaged over 31 years and respective anomaly (third column) over the Indian land region.

Figure 3: Spatial distribution of trend in SW, LW ( $\text{Wm}^{-2}\text{yr}^{-1}$ ) and high and low cloud fraction. Top panel is for MERRA and lower panel for CFSR

Figure 4: Annual surface energy budget averaged over 1979 – 2009. Cloud fraction (1979-2009) and AOD (2000-2009) is presented on right Y axis

Figure 5: Annual bias (CFSR –MERRA) in the surface energy budget fluxes averaged over 1979 – 2009.

Figure 6: Annual cycle of aerosol and cloud Effect averaged over 1979 – 2009.

Figure 7: Relationship between high cloud fraction bias and biases in the fluxes (SW, LW, H, LH) and PBL height.

Figure 8: Relationship between low cloud fraction bias and biases in the fluxes (SW, LW, H, LH) and PBL height.

Figure 9: Latitudinal distribution of cirrus reflectance from MODIS dataset averaged over Indian region from 2001 to 2005 JJAS. Error bars give the standard deviation.

Figure 10: Anomaly of cloud water over regions R2 (a) and R3 (b) and cloud ice mixing ratios over

R2 (c) and R3 (d).

Figure 11: Bowen ratio relationship with cloud and aerosol effect anomaly.

**Table captions:**

Table I: Annual radiative fluxes at the surface averaged over 31 years in  $Wm^{-2}$

Regions	Net SW (down - up)	Net LW (up - down)	SH	LH	GH
R1	194	89	54	50	-0.031
R2	191	73	41	75	-0.055
R3	200	71	49	78	-0.012
R4	195	58	44	91	-0.053

Table II: Maximum attenuation in SW and LW fluxes due to aerosol and clouds ( $Wm^{-2}$ ).

Region	Aerosol effect on SW	Aerosol effect on LW	Cloud effect on SW
R1	-24.5	-9.82	-86.31
R2	-25.3	-6.87	-112.91
R3	-19.02	-4.50	-101.21
R4	-16.29	-1.93	-97.18

Table III: Observed trend in High and Low cloud cover (in percent) for MERRA and CFSR.

MERRA values are significant at 95% . CFSR values are significant at 80% . Numbers with an \* represent not significant.

Region	Seasons	High Clouds (MERRA)	High Clouds (CFSR)	Low Clouds (MERRA)	Low Clouds (CFSR)
R1	Annual	0.23	0.08*	0.07	-0.05
	Pre-monsoon	-0.07*	-0.04*	0.03	-0.02*
	Monsoon	0.62	0.23*	0.25	0.05*
R2	Annual	0.20	0.07	0.16	-0.06
	Pre-monsoon	0.22	-0.01*	0.08	0.01*
	Monsoon	0.23	0.22*	0.32	0.03*
R3	Annual	0.30	0.31*	0.08	-0.07
	Pre-monsoon	0.39	0.05*	0.14	0.06*
	Monsoon	0.30	0.01*	0.11	0.02*
R4	Annual	0.04	-0.05*	0.26	0.04
	Pre-monsoon	0.13	0.09	0.46	0.10
	Monsoon	-0.04	-0.23	0.09	0.07

Table IV: Observed trend in SW and LW flux for MERRA and CFSR in  $\text{Wm}^{-2} \text{yr}^{-1}$ .

MERRA values are significant at 95% . CFSR values are significant at 80% . Numbers with an \* represent not significant.

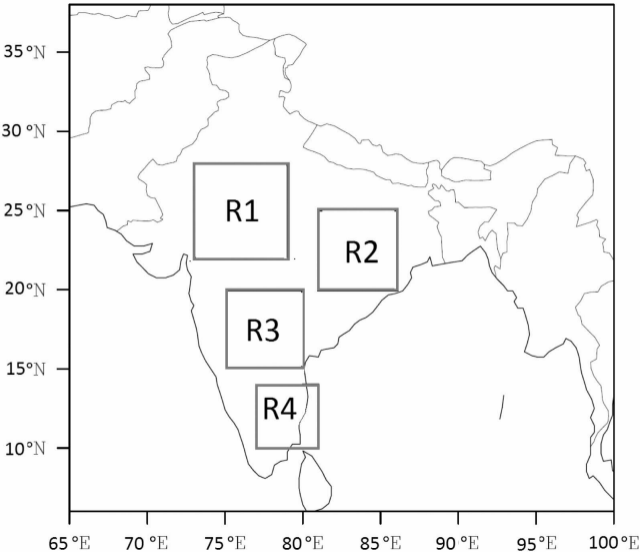
Region	Seasons	SW (MERRA)	SW (CFSR)	LW (MERRA)	LW (CFSR)
R1	Annual	-0.48	+0.07*	-0.42	-0.03*
	Pre-monsoon	-0.16	+0.09*	-0.24	+0.10*
	Monsoon	-1.28	-0.15*	-0.72	-0.16
R2	Annual	-0.59	+0.04*	-0.43	-0.01*
	Pre-monsoon	-0.53	-0.03*	-0.67	-0.04*
	Monsoon	-1.09	-0.05*	-0.40	-0.09
R3	Annual	-0.64	-0.07	-0.41	+0.07
	Pre-monsoon	-0.73	+0.05	-0.78	-0.04*
	Monsoon	-1.04	-0.05*	-0.35	+0.05*
R4	Annual	-0.57	+0.1	-0.39	-0.11
	Pre-monsoon	-1.23	0.28	-0.80	-0.28
	Monsoon	-0.39	-0.01*	-0.23	-0.01*

Table V: Observed trend in Sensible Heat (H), Latent Heat (LH), Bowen Ratio (B) and PBL height over all regions in  $\text{Wm}^{-2} \text{yr}^{-1}$ . MERRA values are significant at 95% . CFSR values are significant at 80% . Numbers with an \* represent not significant.

Region		H		LH		PBL Height	
		MERRA	CFSR	MERRA	CFSR	MERRA	CFSR
R1	Annual	-0.59	+0.03*	0.52	0.02*	-4.48	-0.15*
	Pre-monsoon	-0.122	+0.06	0.31	-0.03*	-1.69	-1.90
	Monsoon	-0.95	-0.16*	0.41	0.19*	-7.02	-1.45*
R2	Annual	-0.49	-0.001*	0.31	0.07*	-3.98	-0.93
	Pre-monsoon	-0.71	-0.02*	0.89	0.01*	-5.67	-0.56*
	Monsoon	-0.47	-0.11*	-0.23	0.15*	-3.91	-0.69*
R3	Annual	-0.52	-0.12	0.28	-0.01*	-3.65	-0.34*
	Pre-monsoon	-0.85	-0.04*	0.95	0.10	-6.37	-1.40
	Monsoon	-0.59	-0.19*	-0.12*	-0.04*	-4.13	-1.68
R4	Annual	-0.71	0.02*	0.67	-0.10	-4.33	-0.75
	Pre-monsoon	-1.48	0.16	1.27	-0.05*	-5.81	-1.02
	Monsoon	-0.72	-0.07*	0.58	-0.31	-4.11	-0.60*

Table VI: Observed correlation between aerosol effect (AE) and cloud effect (CE) with Bowen ratio, where R is correlation coefficient (Figure 11).

Region		Annual		Pre- monsoon		Monsoon	
		Slope	R	Slope	R	Slope	R
<b>R1</b>	AE	-0.24	- 0.76	- 0.001	- 0.30	- 1.24	- 0.85
	CE	-16.29	- 0.87	- 0.16	- 0.54	- 76.35	- 0.87
<b>R2</b>	AE	-1.04	- 0.75	- 1.04	- 0.75	- 3.81	- 0.79
	CE	- 45.35	- 0.84	- 45.35	- 0.83	- 151.53	- 0.78
<b>R3</b>	AE	- 0.27	- 0.38	- 0.04	- 0.67	- 0.25	- 0.15
	CE	-53.29	- 0.88	- 4.02	- 0.88	- 154.85	- 0.85
<b>R4</b>	AE	- 0.25	- 0.58	- 0.16	- 0.82	+ 0.04	+ 0.04
	CE	- 33.64	- 0.82	- 13.42	- 0.79	- 42.87	- 0.77

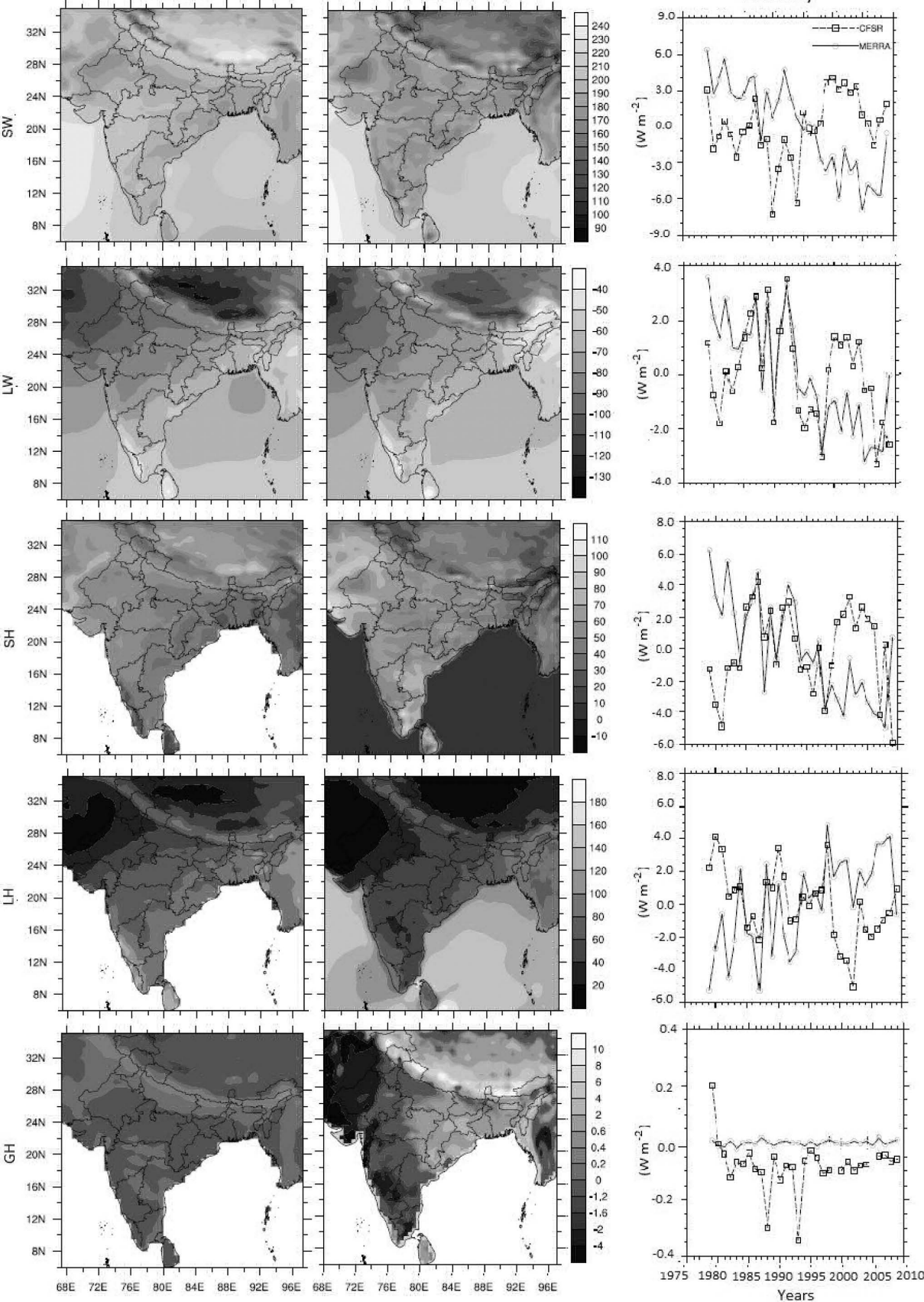




MERRA

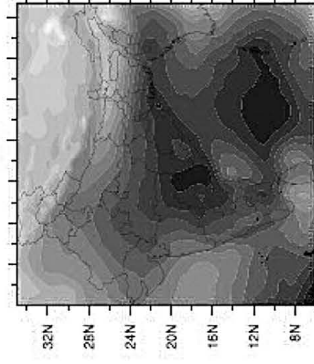
CFSR

Anomaly

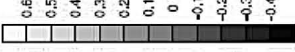
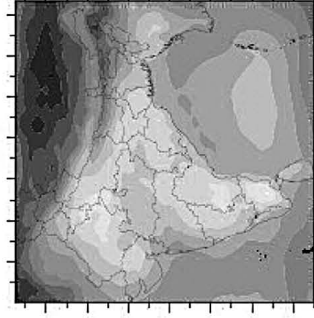


Years

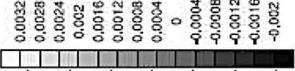
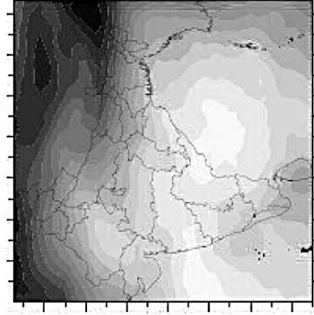
SW



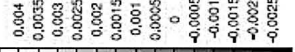
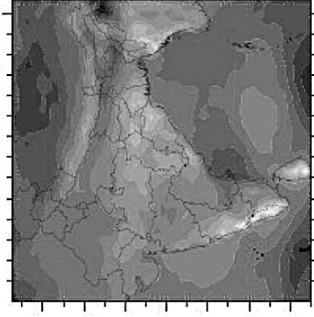
LW



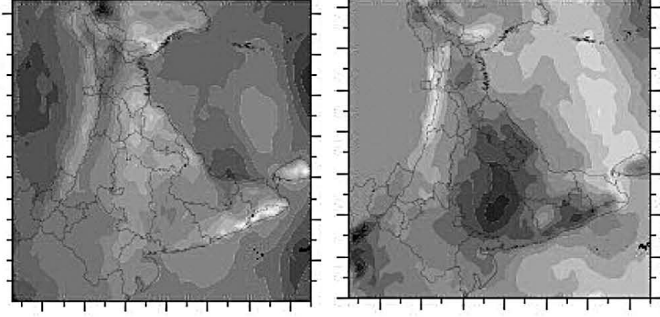
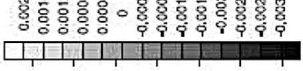
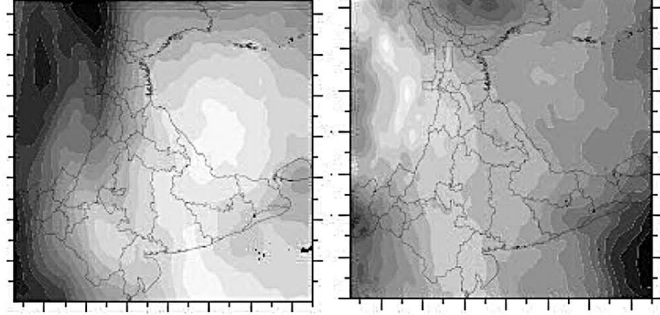
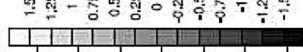
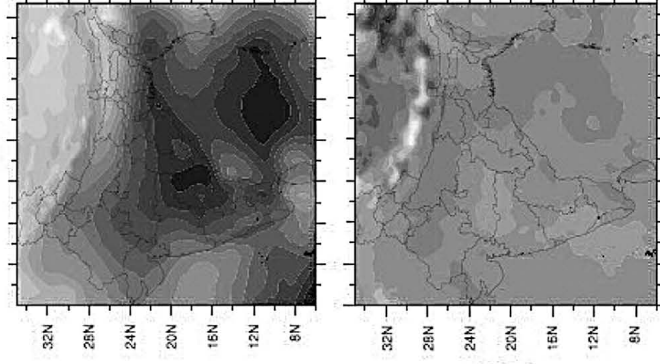
High Clouds

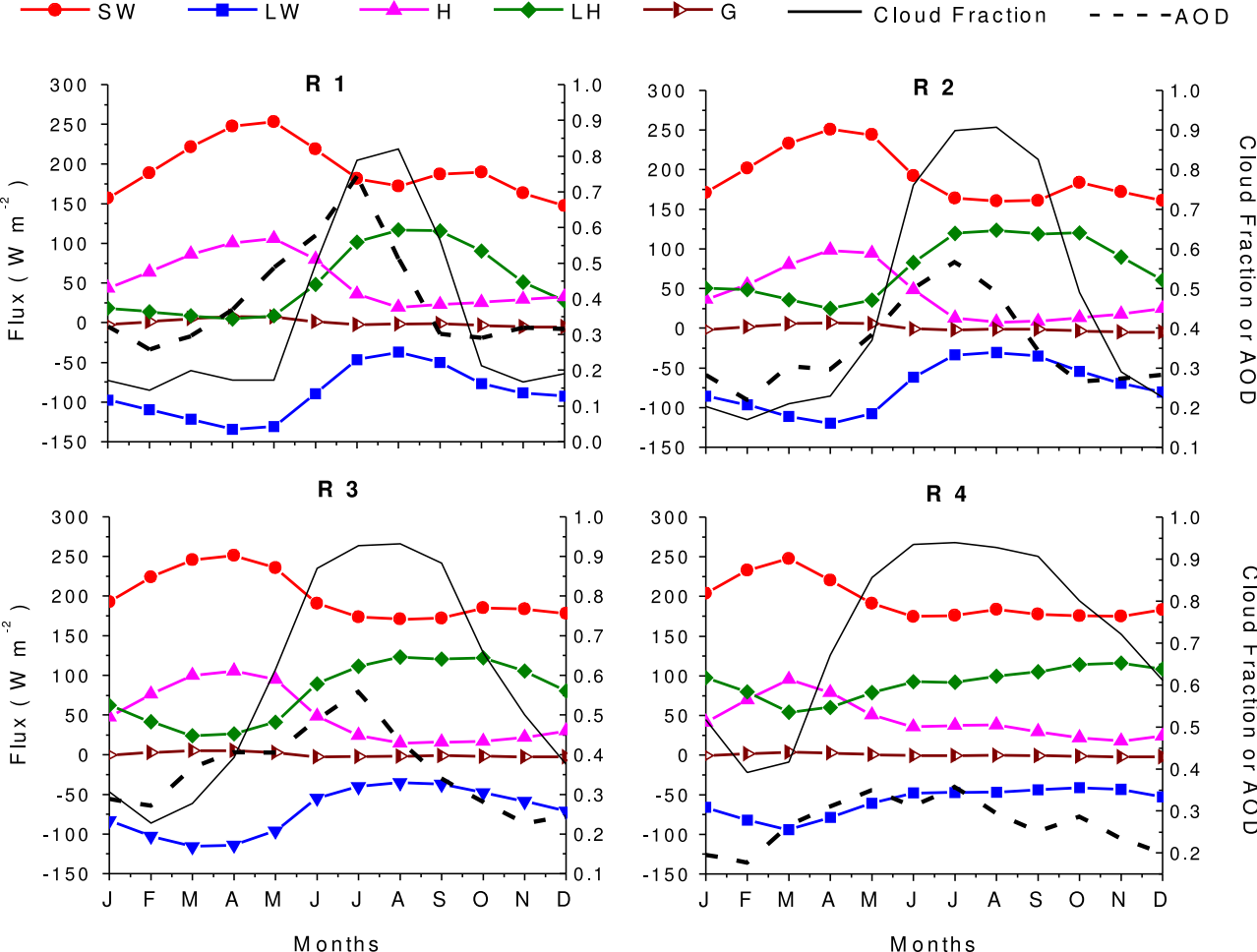


Low Clouds

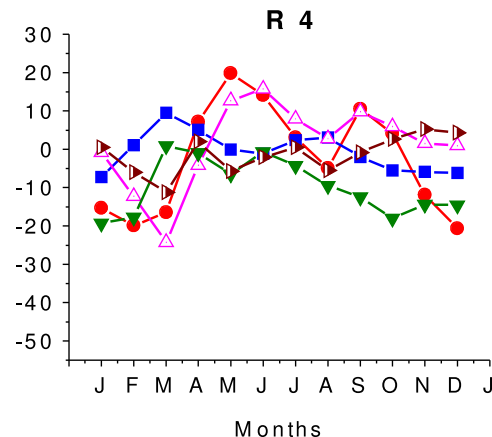
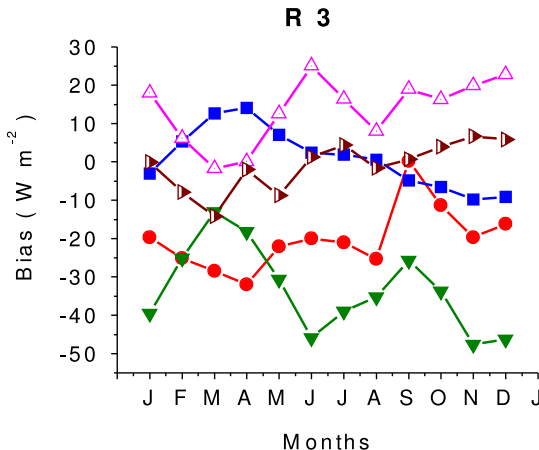
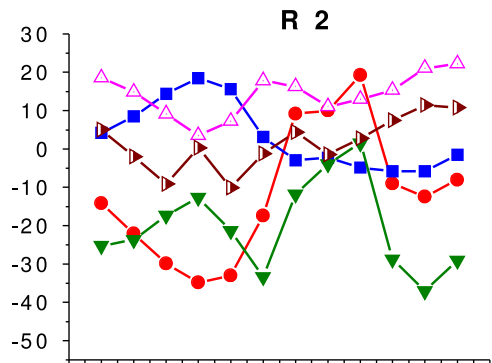
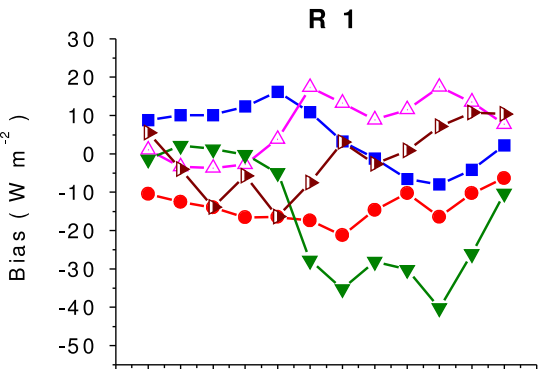


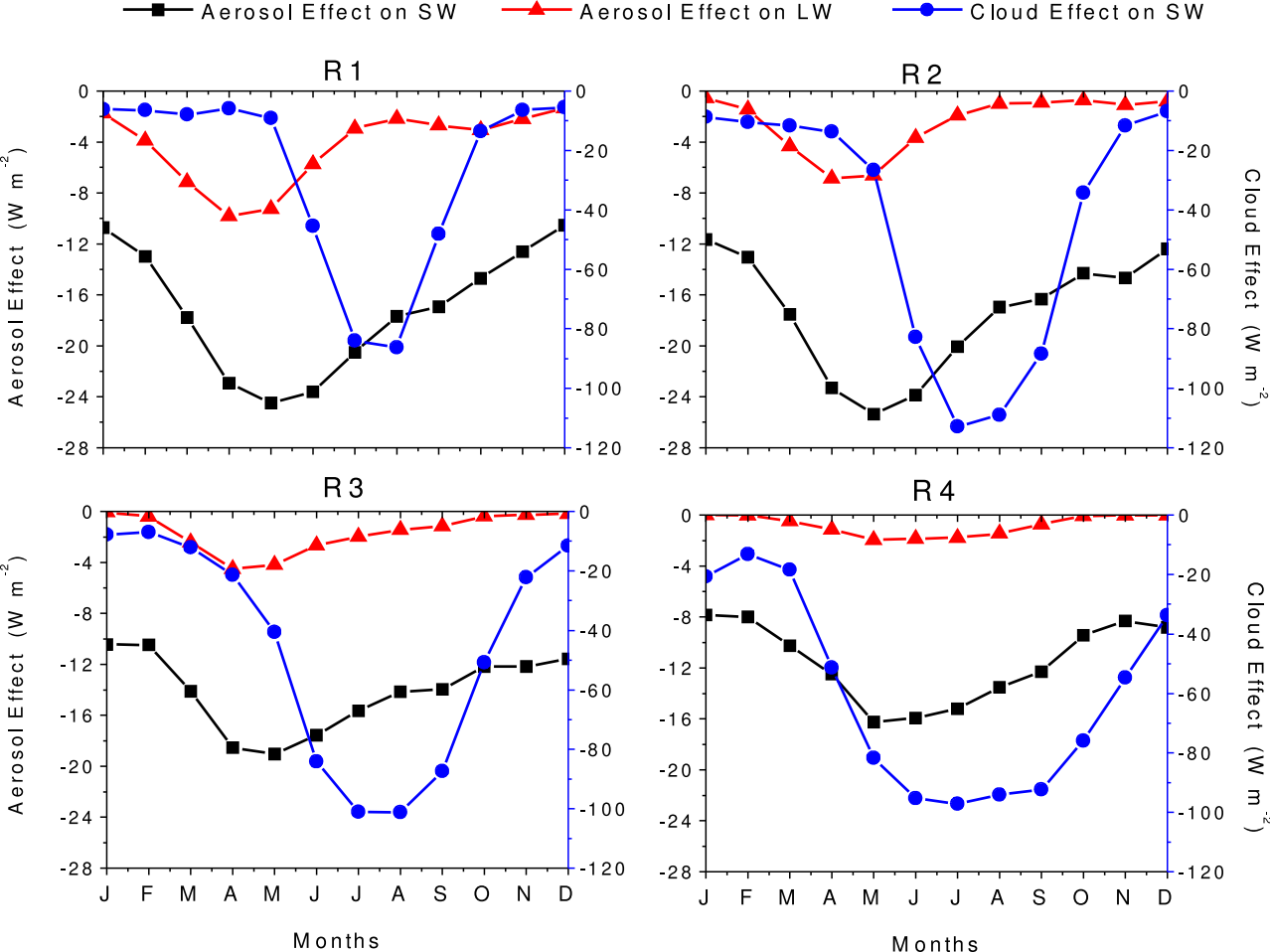
CFRSR





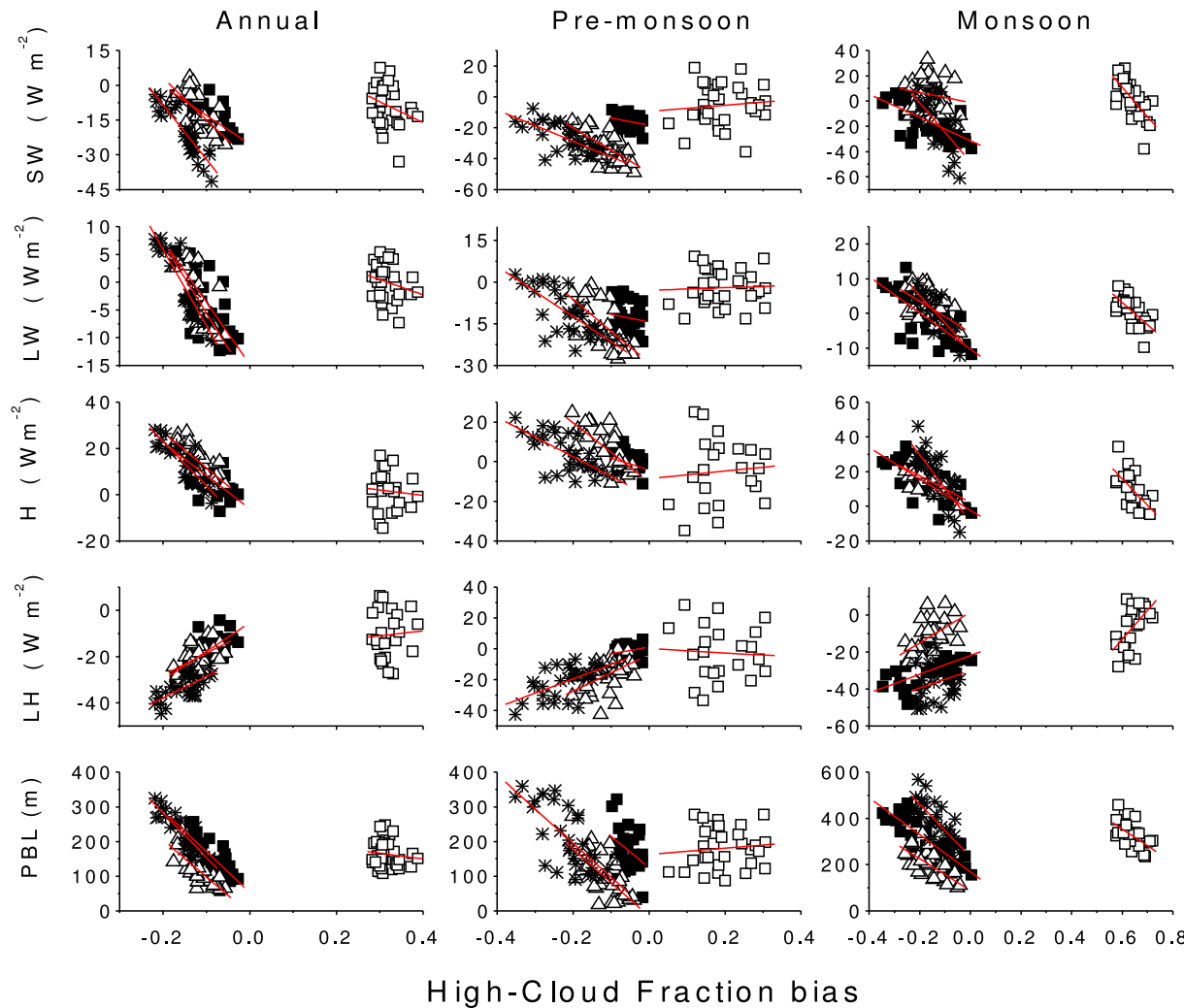
—●— SW    —■— LW    —△— H    —▽— LH    —▷— G





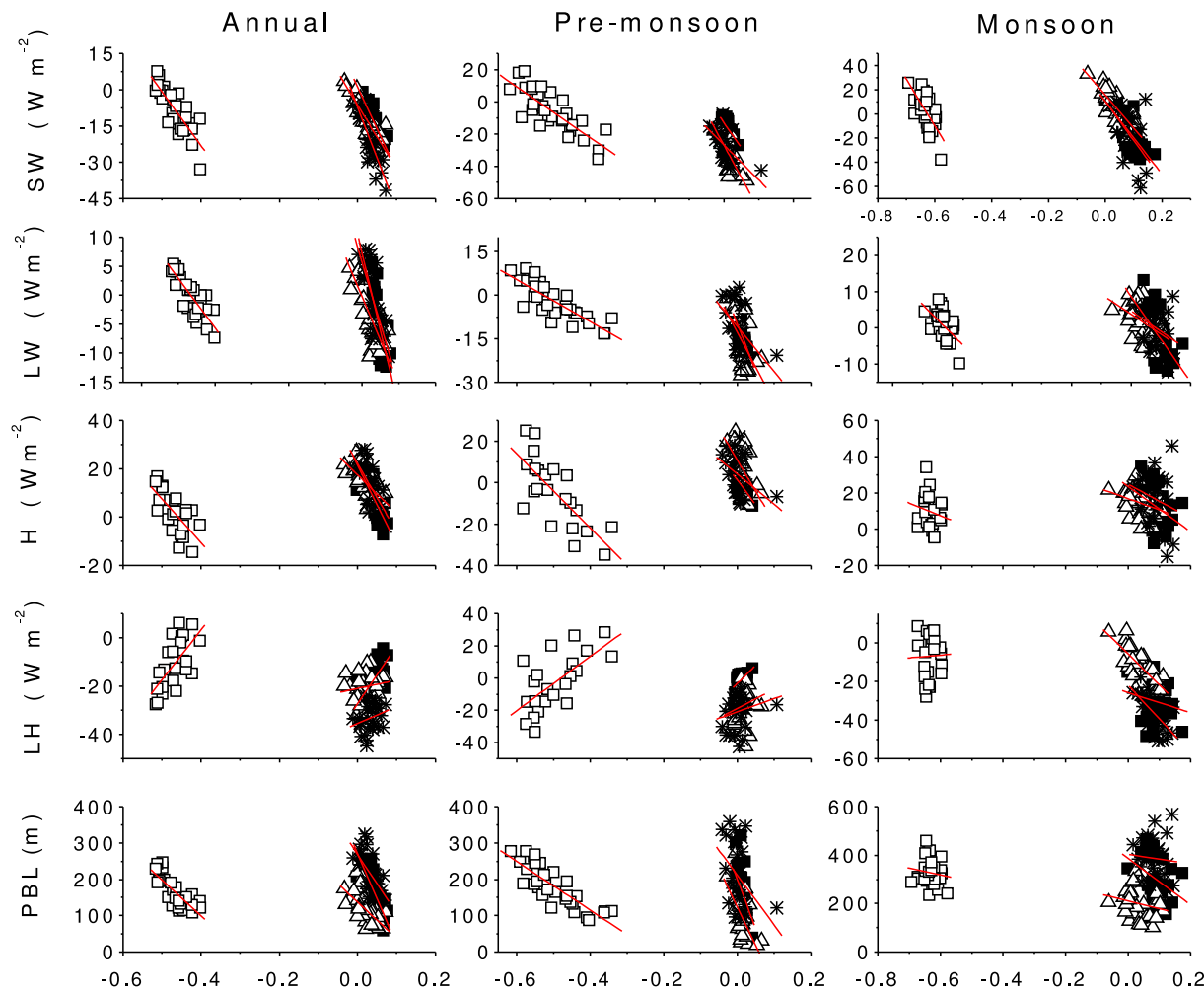
■ R1    △ R2    \* R3    □ R4

Bias

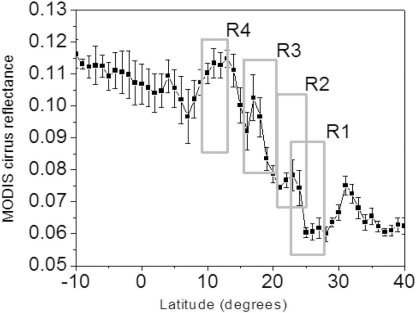


■ R1    △ R2    \* R3    □ R4

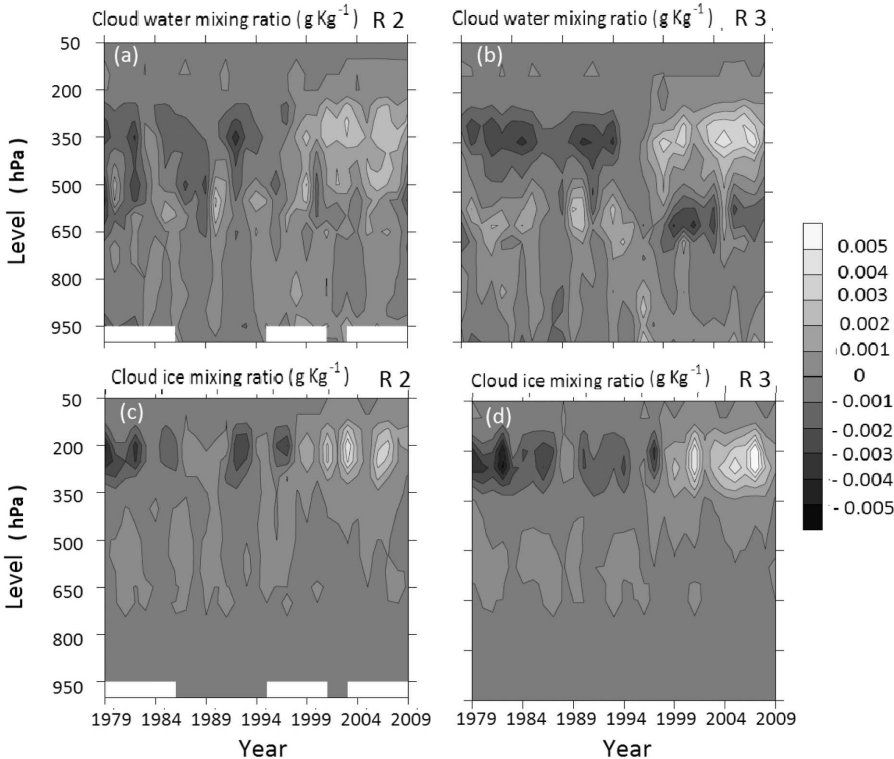
Bias



Low-Cloud Fraction bias







□ Aerosol effect ● Cloud effect

